Thermal Imaging of Afterburning Plumes

E. Ajdari,* E. Gutmark,† T. P. Parr,‡ K. J. Wilson,§ and K. C. Schadow¶
Naval Weapons Center, China Lake, California 93555

Afterburning and nonafterburning exhaust plumes were studied experimentally for underexpanded sonic and supersonic conical circular nozzles. The plume structure was visualized using thermal imaging and regular photography. Thermal emission by the plume is mainly dependent on the presence of afterburning. Temperature and reducing power (or unoxidized fuel content) of the exhaust gases, in addition to the nozzle configuration, determine the structure of the plume core, the location where the afterburning is initiated, its size, and intensity. The temperature, through chemical kinetics, determines the presence of afterburning and its initiation location. Its effect is especially critical in marginally afterburning plumes. The fuel content determines the size and intensity of the plume when afterburning occurs. Comparison between single shot and average thermal images of the plume show that afterburning is a highly turbulent combustion process.

Introduction

THERMAL imaging of rocket motor plumes is a versatile and handy tool to analyze the complex flow dynamics and combustion processes involved in the mixing of hot fuel-rich jets with air.

A rocket plume flowfield is composed of a core surrounded by a mixing layer. The core of the plume contains the unmixed exhaust gases. Its structure is determined by inviscid gasdynamics that depend strongly on the pressure at the nozzle exit. Improperly expanded gas results in a complex shock structure embedded in the core, which affects the temperature distribution along the plume.

Surrounding the core region is a viscid mixing region, where the combustion gases mix with the atmospheric gases. This mixing process depends on the turbulent flow dynamics of a compressible shear layer. This process can result in afterburning of the exhaust gases in the turbulent mixing layer. In order to obtain this secondary combustion, several conditions should be met: 1) the exhaust gases should contain a certain amount of unoxidized fuel (reducing power); 2) the fluid dynamics need to supply the proper mixing with ambient air; and 3) the ignition temperature has to be reached. Various modeling techniques use inviscid gasdynamics mixing processes to study these conditions and to predict the spatial distribution of temperature and species concentration. These studies show that turbulent mixing processes play an important role in the accuracy of the modeling.[1]

The present work studies these processes experimentally. It is part of a more comprehensive program to study the interaction of combustion and flow dynamics in supersonic jets. In earlier works, we looked into this interaction in sonic underexpanded circular jets and studied the effect of the acoustic near-field on the jet structure.[2,3] The mean and turbulent flowfields of sonic and supersonic jets were studied with free and coaxial flows. These studies showed that through acoustic feedback from shock/shear layer interaction,[4] the jet structure is highly sensitive to the exit conditions. Excitation of the axisymmetric or helical modes significantly varies the jet's spreading rate and its turbulence level.

Presented as Paper 89-0062 at the AIAA 27th Aerospace Sciences Meeting, Reno, NV, Jan. 9–12, 1989; received July 5, 1989; revision received Feb. 2, 1990.

*Visiting Scientist, Research Department.
†Research Scientist, Research Department. Member AIAA.
‡Research Chemist, Research Department.
§Aerospace Engineer, Research Department.
¶Supervisory General Engineer, Research Department. Member AIAA.

The present paper describes reacting tests performed with afterburning and nonafterburning plumes. The test facility enabled control of the exhaust gas composition, the exit plane temperature, and velocity. Thus, the effect of these parameters on the afterburning process could be investigated in sonic underexpanded and supersonic fully expanded plumes. Thermal images as well as regular photographs were analyzed for the different conditions.

Experimental Arrangement

A gas generator burning ethylene, air, oxygen, and nitrogen was used to produce the plume (Fig. 1). The pressure inside the gas generator was kept constant at $P_{CH} = 150$ psi (1.03 MPa). The initial conditions in the plume at the nozzle exit were varied by changing the composition of the gases in the combustion chamber.

Two nozzles were used at the outlet of the gas generator to obtain sonic and supersonic plumes. The sonic nozzle had only a contraction section with an exit diameter D of 1.9 cm. The supersonic nozzle had conical contracting and diverging sections. The design Mach number at the exit was 2.38. The throat diameter was 1.9 cm, the exit diameter 2.92 cm, and the conical divergence angle was 16 deg.

The parameters chosen to describe the test conditions are the nozzle type (super/sonic) and the jet exit temperature and reducing power (sum of the mole fraction of H_2 and CO, or the unoxidized fuel content in the plume). Temperature and composition of the exhaust were computed from the pressure

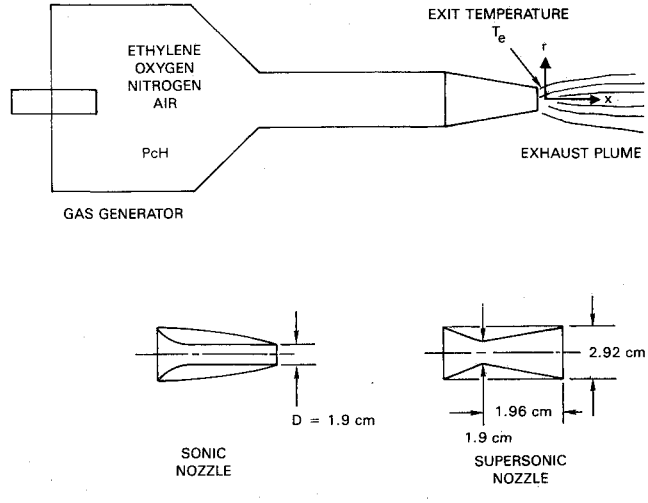

Fig. 1 Experimental setup.

and the composition of the gases in the combustion chamber using a thermochemical program for propellant evaluation. Isentropic expansion from chamber pressure to ambient with chemical equilibrium was assumed. Reducing power was preferred to equivalence ratio to describe the test conditions since the latter is more relevant to the analysis of the combustion in the chamber, while the former describes the amount of chemical species that may afterburn in the plume. The test conditions are summarized in Table 1.

The radiance intensity of the plume was measured using a thermal imaging camera, AGA Model 750 Thermovision. This camera has a single detector element that scans the object in a raster pattern containing 74 active lines at a rate of 25 frames per second. Each line contains 100 resolution elements. All optical elements are wideband antireflection coated. The camera, equipped with a narrow band filter, was operated at a spectral band of 4.1-4.9 μm. The distance from the camera to the plume was changed in the tests between 0.9 to 12 m, covering a length of 0.12 m for the closeup images of the plume's core region to 1.5 m for a wide field of view of the plume.

The signal from the infrared camera was acquired at 25 frames per second using a custom constructed time corrector with a transient digitizer interfaced to a personal computer. The digitizer allows acquisition of up to 256 frames at once, which are transferred to the PC for immediate color contour display, analysis, and archiving. The image-processing software allows contrast stretching, image smoothing and edge detection, and linear graphs over user-chosen rectilinear subregions. It also allowed us to compute total radiance averaged over a user-chosen subregion of the total image. It supports color and grey scale hardcopy output. All of the distance in the figures are nondimensionalized by the nozzle throat diameter. For the isoradiance contours, axial and radial length scale are identical.

The camera was calibrated for spectral response, responsivity, and field of view. The spectral response is measured using a monochromator. The camera and the thermocouple of the monochromator share a narrow spectral band output beam (<0.03 μm), and the signals are ratioed over the wavelength region being used. The optical paths from the source to the thermocouple and camera are purged with dry nitrogen to reduce atmospheric absorption.

The responsivity of the camera is determined by placing a calibration source in the field of view. A 2.54-cm-diam conical cavity source was used at the focal plane of a 0.625 focal length off-axis collimator. At the calibration range, most of the collimator appears to have the radiance of a blackbody cavity less some insertion loss. The temperature readout of a high-temperature source is calibrated against an NBS traceable thermocouple inserted into the cavity.

Knowing the spectral response of the imaging radiometer, and estimating losses due to atmospheric transmission from the local climatic conditions, the effective radiance of the calibration source can be calculated. Denoting this radiance by E^o and the corresponding voltage level by V^o, the measured radiance E is related to the measured voltage V by the equation:

$$E = \frac{V - V_{off}}{V^o - V_{off}} E^o$$

where V_{off} is the offset voltage. This offset voltage can be arbitrarily adjusted to cover the full dynamic range of the analog to digital converter.

In addition to the thermal images, the plume was photographed by a regular camera and recorded on a videotape.

Results and Discussion

Firing Conditions and Observation of Afterburning

The tests are categorized in two groups: 1) afterburning plumes and 2) nonafterburning plumes (see Table 1). This condition was determined from the thermal images except for tests 8 and 9 for which color photographs were used. Figure 2 displays the test conditions for the sonic underexpanded plumes and the supersonic ones in a reducing power vs temperature diagram. Reducing power was used to indicate the amount of unoxidized fuel content in the exhaust gases. More test conditions are quoted in these diagrams than in Table 1, which contains only the test specifically analyzed in this paper.

Table 1 Test conditions

Test no.	Reducing power, %	Exhaust temperature, K	Nozzle (super/sonic)	Afterburning, (Y/N)
1	18	1170	Sonic	N
2	50	1120	Super	N
3	58	1220	Super	Y
4	19	1440	Sonic	Y
5	35	1330	Sonic	Y
6	16	1190	Super	N
7	55	1170	Super	Y
8	32	1300	Sonic	Y
9	32	1300	Super	N
10	20	1240	Sonic	N
11	21	1230	Super	N
12	17	1180	Sonic	N
13	17	1190	Super	N
14	37	1280	Super	Y
15	33	1260	Sonic	Y
16	37	1290	Super	Y
17	33	1350	Sonic	Y
18	36	1320	Super	Y

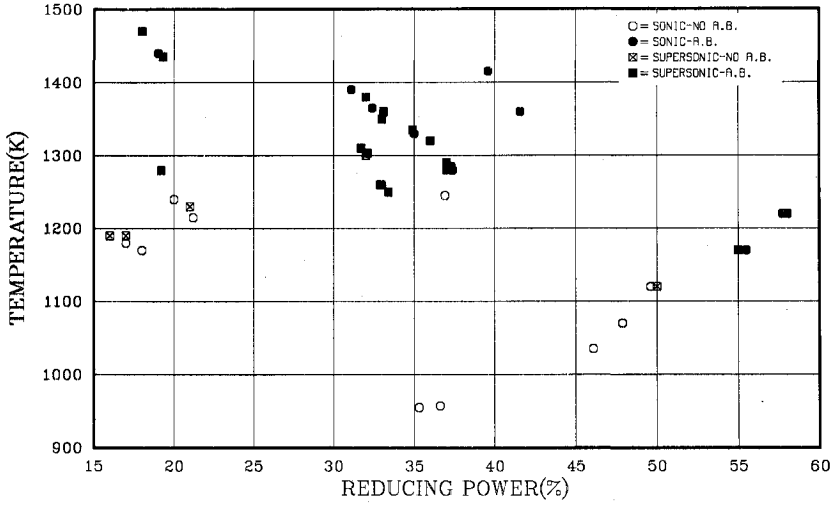

Fig. 2 Test conditions for sonic underexpanded and supersonic plumes.

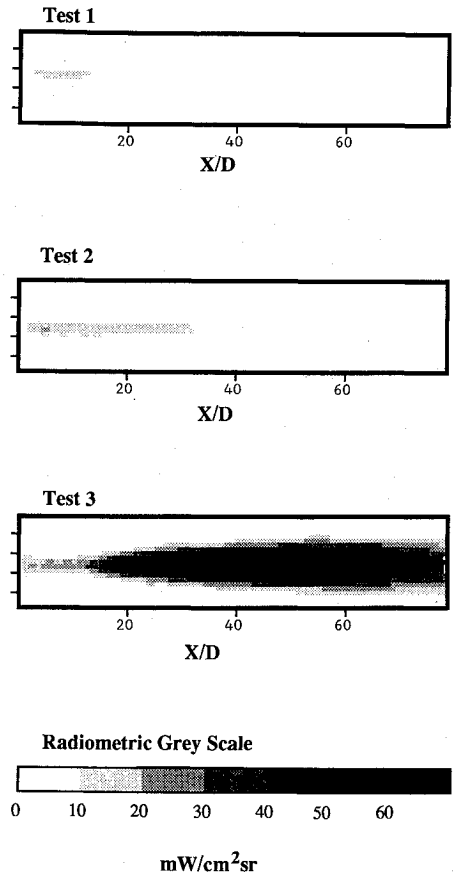

Fig. 3 Average isoradiance contours of three plumes. Test 1: $RP = 18\%$, $T = 1170$ K, sonic nozzle, no afterburning; test 2: $RP = 50\%$, $T = 1120$ K, supersonic nozzle, no afterburning; and test 3: $RP = 58\%$, $T = 1220$ K, supersonic nozzle, afterburning.

Afterburning and nonafterburning regions can be identified in these diagrams. For both the supersonic and sonic plumes, the limit is near 1250 K for the lower range of reducing power and 1150 K for the higher range.

Visual observation and IR pictures show that position and intensity of afterburning flames are fluctuating, especially near the limit of the afterburning region where temporary extinctions are observed. This phenomenon will often be referred to in this paper as marginal afterburning. In some cases, such as test 14, most of the IR pictures do not show any afterburning, and the assessment of the presence of afterburning is not obvious. Moreover, very small changes in the test conditions (like from test 14 to test 16) can cause dramatic changes in the plume. (These two tests are analyzed further in the paper.)

Influence of Afterburning on Plume IR Emissions

The amount of IR radiation emitted by the exhaust plume is mainly dependent on the presence of afterburning in the plume. Figure 3 shows the average thermograms (isoradiance contour in w/cm²sr) of tests 1–3. Afterburning was present in test 3, but not in tests 1 and 2. The test conditions of tests 1 and 2 are very different, whereas they are relatively similar between tests 2 and 3. However, the difference in emitted radiation between tests 1 and 2 is very small compared to the difference between tests 2 and 3. The total emitted IR radiation in test 3 is more than 20 times larger than in test 2, which emits only three times as much as test 1. Actually, the difference between the afterburning plume and the nonafterburning ones is even greater since plume radiation outside the field of view of the camera is not considered.

In the following sections, the different factors that affect afterburning will be discussed.

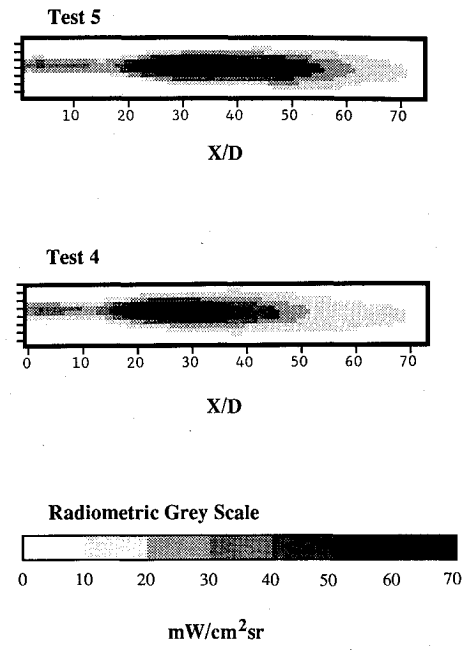

Fig. 4 Average isoradiance contours of two afterburning sonic underexpanded plumes. Test 4: $RP = 19\%$, $T = 1440$ K; and test 5: $RP = 35\%$, $T = 1330$ K.

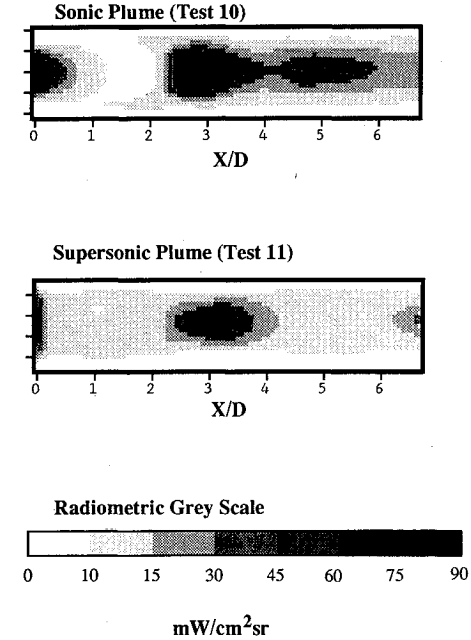

Fig. 5 Average isoradiance contours of two nonafterburning plumes (closeup). Test 10: sonic plume; and test 11: supersonic plume.

Effect of Exit Temperature and Reducing Power on Afterburning: Influence of Chemistry

Starting from conditions for which the plume does not afterburn (test 1 or 6), afterburning can be obtained by increasing the reducing power (test 7) or by increasing the temperature (test 4).

Afterburning occurrence seems to be more sensitive to changes in temperature than in reducing power, as can be expected in a process where chemical kinetics is important. Indeed chemical reaction rates usually follow an Arrhenius-type law, where temperature appears in the exponential factor, whereas species concentration is only a linear factor. Chemical kinetics will also affect the location of the upstream end of the flame and its size and intensity. However, for conditions pro-

ducing good afterburning, the latter is more dependent on the thermochemistry of the exhaust/air mixing, which defines the maximum releasable energy and is primarily determined by the reducing power.

This point is illustrated in Fig. 4, where two afterburning plumes are compared. The temperature is higher for test 4, and therefore the position of the upstream edge of the flame, which is determined by the chemical kinetics in addition to fluid dynamics, is closer to the nozzle. The reducing power is higher for test 5, which thus has a longer and more emissive afterburning flame. The distance between the nozzle exit and the upstream edge of the plume region emitting more than 30 mW/cm^2/sr—in black in Fig. 5—is 15 nozzle diameters (15D) for test 4 vs 21D for test 5. The length of this region is, respectively, 22D vs 27D.

Effect of the Nozzle Shape on Afterburning: Influence of Fluid Dynamics

The use of a sonic nozzle instead of a supersonic one has a significant influence on afterburning. Sonic underexpanded plumes afterburn at a lower temperature (with a constant reducing power) or at a lower reducing power (with a constant temperature) than supersonic fully expanded ones. An example for this case is given by tests 8 and 9 with identical temperature (1300 K) and reducing power (32%) but different nozzles. In test 8 (sonic nozzle), an afterburning flame was visible starting 9D downstream from the nozzle, extending to 20D, whereas no afterburning was present in test 9.

In order to analyze the differences in the plume structure due to the nozzle configuration, the camera was set close to the plume (0.9 m) so that the field of view covered only 7D of the plume downstream from the nozzle. The results are shown in Fig. 5 for nonafterburning conditions.

In the sonic underexpanded plume, the shock structure in the core is evident. The initial high temperature, which is indicated by the high level of radiance, is cooled down below the exit temperature of the supersonic plume, followed by a rapid temperature increase downstream of the Mach disk. A weaker shock cell is visible downstream.

For the supersonic plume, a shock structure is also apparent, although the nozzle was operated in fully expanded conditions, as a result of the conical diverging section of the nozzle. The shocks are oblique and much weaker relative to the sonic underexpanded plume, and the second shock cell appears farther downstream.

In Fig. 6, the axial IR emission profiles of two nonafterburning plumes exiting from sonic and supersonic nozzles are compared on a larger field of view (40D). The slightly different test conditions do not affect this analysis.

The sonic underexpanded jet mixes faster with the ambient air than the supersonic one. Its axial IR emission, initially higher than that of the supersonic plume, drops below beyond 15D with a complete damping of the shock cell oscillations. The shock cell structure of the supersonic plume is still detectable 25D downstream, showing that the flow there is still supersonic.

Keeping the same field of view, the test conditions were changed to obtain afterburning. Axial radiation plots from single shot (duration) and average images are shown in Fig. 7 for a supersonic plume and Fig. 8 for a sonic plume.

The flame starts closer to the nozzle and is more intense in the sonic plume than in the supersonic one, although the exit temperature and reducing power are slightly lower, thus less in favor of afterburning. This is probably the consequence of higher initial jet core temperature and possibly larger mixing in the sonic underexpanded plume. The large variability of the

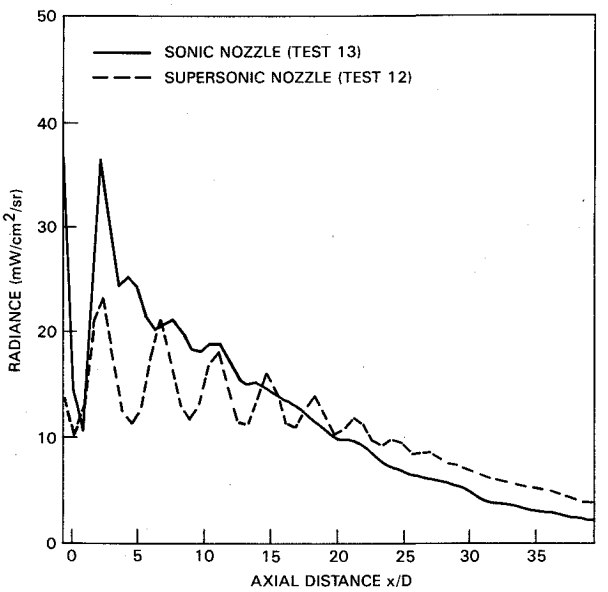

Fig. 6 Average centerline radiance profiles of two nonafterburning plumes. Test 12: sonic plume; and test 13: supersonic plume.

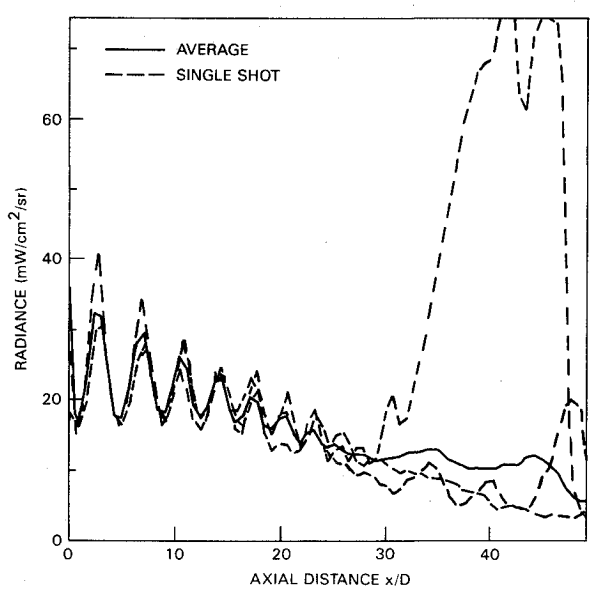

Fig. 7 Single-shot and average centerline radiance profiles of a supersonic plume with marginal afterburning (test 14).

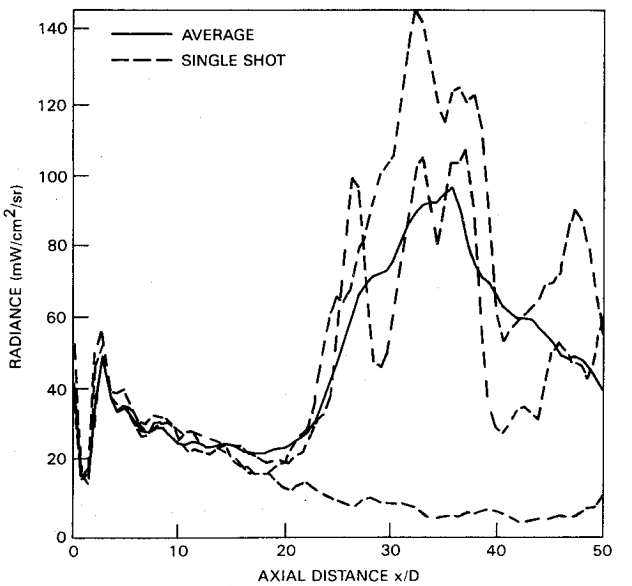

Fig. 8 Single-shot and average centerline radiance profiles of a sonic underexpanded plume with marginal afterburning (test 15).

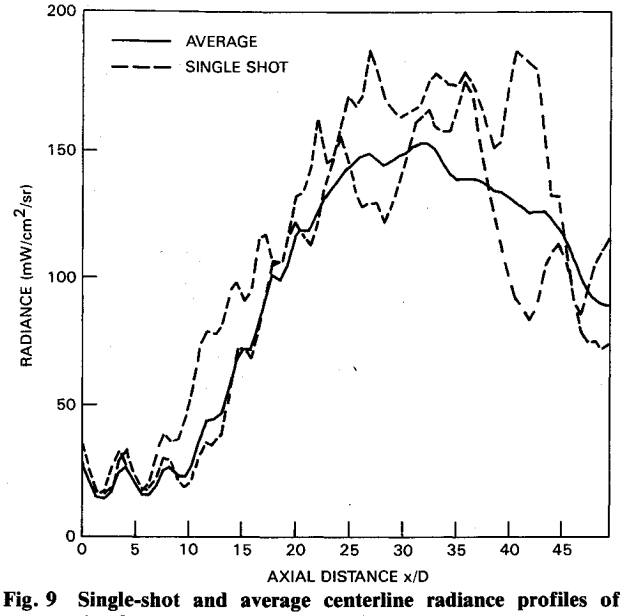

Fig. 9 Single-shot and average centerline radiance profiles of a supersonic afterburning plume (test 16).

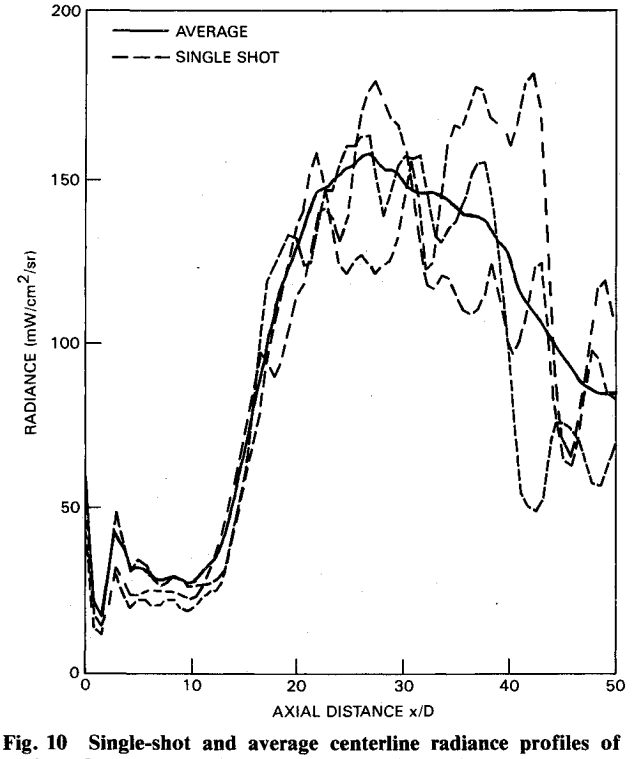

Fig. 10 Single-shot and average centerline radiance profiles of a sonic underexpanded afterburning plume (test 17).

single-shot profiles show that the afterburning flame is highly unstable and turbulent, with large differences in the emission profile and occasional complete absence of afterburning. The shock cell periodic structure in the supersonic plume has some amplitude fluctuation in some frames, probably due to the interaction between shock cell instabilities and turbulent combustion.

A small temperature increase stabilizes and strengthens afterburning in the supersonic plume (Fig. 9). It can be observed that the flame starts closer to the nozzle exit within the supersonic part of the plume. The shock cell's structure is still visible in both the single-shot and average profiles inside the afterburning flame. The local temperature maxima in the shock cells act as flameholders for the afterburning. Because

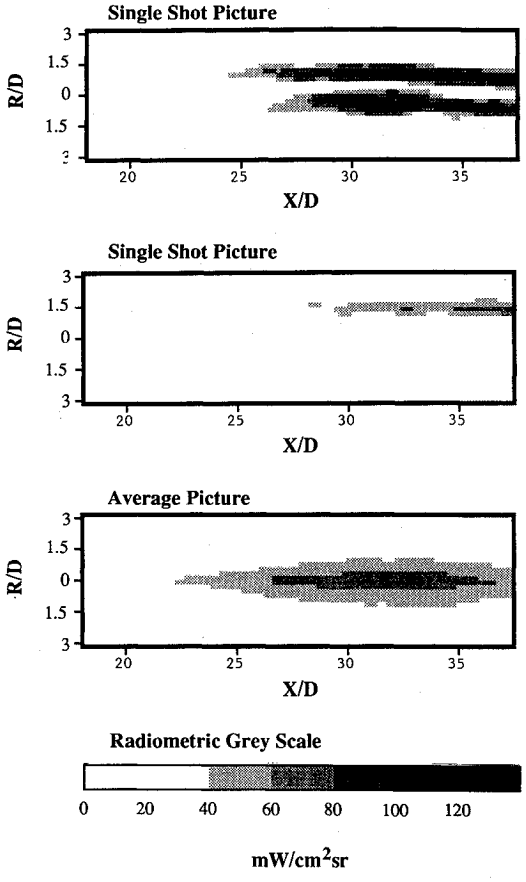

Fig. 11 Average and single-shot isoradiance contours of an afterburning flame (closeup of test 18).

of the turbulence, the flame starts randomly at the second or third shock cell, as seen in the single-shot profiles.

In the sonic underexpanded plumes, afterburning occurs in the subsonic region where the inviscid shock structure of the plume has disappeared. Although afterburning still appears to be a highly turbulent process, the starting location of the flame is less dispersed than in the supersonic plume (Fig. 10).

Turbulence in Afterburning Flame. Limitations of the Average Steady-State Analysis

Single-shot IR pictures show that the radiance intensity in the afterburning flame has a random distribution both spatially and temporally. Averaging the picture results in smoothing the flame structure and reducing the peak radiance intensity. Peak values in single shots can be two times higher than the average pictures in stable afterburning flames and five times higher in marginal afterburning flames. The differences are maximized in the case of marginal afterburning, since the process is alternating between afterburning and nonafterburning, which appears after averaging as weak afterburning.

To emphasize this, two single-shot pictures and an average one of an afterburning flame are shown in Fig. 11. The test conditions were close to test 16. Afterburning is more unstable than in test 16, although the temperature is slightly higher. However, the differences between the tests are not large enough to be significant regarding the limited accuracy in the control of the motor conditions.

The single-shot pictures show that the flame is composed of pockets of burning gases with peak emission off the axis and strong transverse gradients at the interface with the nonburning parts of the plume. On the average, the burning zones of the plume are mixed with nonreacting ones: the average plume is almost symmetric, with smooth transverse gradient and peak values on the axis, although at a much lower level (typically five times less) than in the single-shot pictures.

Conclusions

Thermal radiation of plumes is mainly dependent on the presence of afterburning. The afterburning in a turbulent combustion process is affected by thermochemistry, chemical kinetics, and viscid and inviscid aspects of the plume fluid dynamics.

Plume thermochemistry determines the maximum heat release in the afterburning flame. It is primarily dependent on the reducing power of the exhaust gases and affects the size and intensity of the afterburning flame, for test conditions that ensure stable afterburning.

Chemical kinetics, mainly temperature dependent, will determine the actual heat release in the plume due to finite combustion reaction rates and, therefore, the presence or absence of afterburning, the position of the upstream edge of the flame, and the size and intensity of marginal afterburning flames.

Nozzle configuration determines the mixing rate (viscous plume structure) and pressure field (inviscid plume structure). Sonic underexpanded plumes are characterized by a stronger shock structure near the nozzle exit and a larger mixing rate relative to the supersonic flow. For the supersonic plumes, the conical shape of the diverging section of the nozzle results in the formation of weak shock cells, that would be absent if the nozzle were a contoured DeLaval one. The shock cells damp very slowly and interact with the turbulent afterburning flame. The different flowfield characteristics between supersonic plumes and sonic underexpanded ones result in afterburning enhancement if the supersonic conical nozzle is replaced by the sonic one.

The turbulent nature of the afterburning combustion is obvious in comparing single-shot pictures and average ones, especially in case of marginal afterburning. Marginal afterburning seems to be characterized by the random development of pockets of burning gases in the shear layer while the rest of the plume remains nonreactive. On the average picture, the plume structure is smooth and symmetric with a much lower peak IR emission.

References

[1]Dash, S. M., Pearce, B. E., Pergament, H. S., and Fishburne, E. S., "Prediction of Rocket Plume Flowfields for Infrared Signature Studies," *Journal of Spacecraft and Rockets*, Vol. 17, May-June 1980, pp. 190–199.

[2]Gutmark, E., Schadow, K. C., Wilson, K. J., and Bicker, C. J., "Acoustic Radiation and Flow Instabilities in Low Supersonic, Circular, and Elliptic Jets," *Physics of Fluids*, Vol. 31, Sept. 1988, pp. 2524–2532.

[3]Gutmark, E., Schadow, K. C., and Bicker, C. J., "Mode Switching in Supersonic Circular Jets," *Physics of Fluids*, Vol. 1, May 1989, pp. 868–873.

[4]Gutmark, E., Koshigoe, S., and Schadow, K. C., "Shock Wave/Shear-Layer Interaction in Circular and Noncircular Jets," *Lecture Notes in Engineering*, Springer-Verlag Series, 1991.